ELSEVIER

Journal of Power Sources 85 (2000) 164–171

JOURNAL OF POWER SOURCES

www.elsevier.com/locate/jpowsour

Influence of temperature, current and number of cycles on the efficiency of the closed oxygen cycle in VRLA batteries

D. Pavlov *, S. Ruevski, V. Naidenov, G. Sheytanov

Central Laboratory of Electrochemical Power Sources, Bulgarian Academy of Sciences, 1113 Sofia, Bulgaria

Accepted 22 September 1999

Abstract

An experimental method was created for assessment of the efficiency of the closed oxygen cycle in VRLA cells. It was experimentally established that at 25% compression of the AGM separator the battery life is the longest one. On the other hand, the efficiency of the closed oxygen cycle (COC) is the highest at 20% compression of the AGM. With an increase of the compression the efficiency of the COC decreases because of the decreasing of the number of the channels (pores) along which the oxygen flows can move through the AGM separator. It was established that the polarization of the VRLA cell is mainly determined by the resistance arising at transportation of the oxygen through the AGM. There is an upper limit of the rate of recombination of oxygen that depends on the structure and properties of the AGM. With increase of the temperature the efficiency of the COC and polarization of the VRLA cell decrease. During cycling, the properties and structure of the AGM change that affects the parameters of VRLAB.

Keywords: Temperature; Closed oxygen cycle; VRLA batteries

1. Introduction

The processes taking place during charge of the lead-acid battery can be divided into three stages: first — an efficient charge stage. Only reactions of charging of the positive and negative plates proceed. The second stage of mixed reactions — water decomposition proceeds parallel to the charge reactions. The third stage is the overcharge stage of water decomposition. The charging reactions are completed and only water decomposition occurs.

The second stage begins when evolution of oxygen starts at the positive plates. At a current of 0.1 C_{20} A, this process begins when the battery has reached about 70–75% state of charge. At 95% state of charge, hydrogen evolution begins. This mismatch of the two processes was utilized by McClelland and Devitt from GATES [1] to create a closed oxygen cycle (COC) in the cell and thus eliminate the need to top up lead-acid batteries (LAB) with water during operation in the field. For the purpose, they inserted absorbing glass mat (AGM) separators between the positive and the negative plates and thus forced the released oxygen towards the negative plates where it was reduced and recombined to water again. The reduction of O_2 stopped the increase in potential of the negative plates thus avoiding hydrogen evolution.

Nowadays, the transport of O_2 towards the negative plates is realized in two ways: first, and most commonly used, through the AGM separator and second, through cracks in gelled electrolyte. Thus, the VRLA batteries have been created, which are winning ever-increasing positions on the battery market.

The reactions that take place during charge of VRLA batteries are presented schematically in Fig. 1.

At the positive plates, $PbSO_4$ is oxidized to PbO_2 consuming water (reaction 4). When the potential of the electrode reaches a value of 1.3 V, evolution of oxygen starts (reaction 5). As evident from the scheme, water reacts in the positive plate and at the positive plate/AGM interface forming PbO_2 and O_2. Consequently, this interface is subjected to drying out and increasing of the concentration of the H_2SO_4.

At the negative plates, the following reactions occur: $PbSO_4$ is reduced to Pb (reaction 1). The oxygen coming from the positive plate oxidizes the lead forming PbO which reacts with H_2SO_4 and $PbSO_4$ and H_2O are formed (reaction 2). Thus, watering takes place at the Pb/AGM

* Corresponding author.

0378-7753/00/$ - see front matter
PII: S0378-7753(99)00396-1

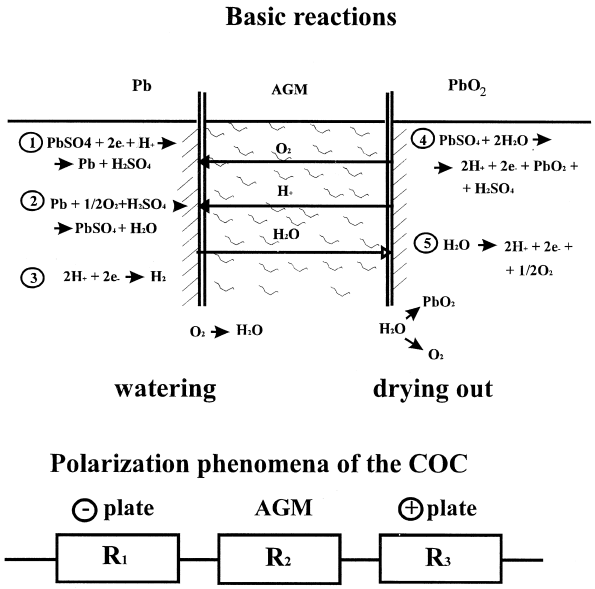

Fig. 1. Scheme of the reactions that take place in the VRLAB.

interface. Under the action of a concentration gradient of the electrolyte between both interfaces of the AGM, the water is directed towards the positive plates and H^+ ions and O_2 flow towards the negative plates. To enable the O_2 flow to move easily towards the negative plates, the AGM separator should have gas channels in its structure. The diffusion coefficient of oxygen is 5 orders of magnitude greater in the gas phase than in the sulfuric acid electrolyte [2]. Therefore, for the COC to proceed, the AGM has to be less than 95% saturated with electrolyte. The other basic reaction at the negative plates is the hydrogen evolution (reaction 3).

Apart from the above reactions, the positive grid undergoes corrosion processes and the expander in the negative active mass (NAM) is oxidized to CO and CO_2. However, these reactions proceed at low rates.

The resistances arising during the course of the COC processes are R_1 at the negative and R_3 at the positive plates. The transport hindrances (R_2) of the H^+, H_2O and O_2 flows moving through the AGM separator play an essential role for the efficiency of the COC. The AGM must be hydrophilic enough to assure easy transport of the H^+ and H_2O flows and must have a low value of R_2. A part of the pores of the AGM must be large enough and free of electrolyte to make the transfer of O_2 through the separator easy. The AGM separators in a VRLA battery contain between 70% and 80% of the electrolyte and the residual 20 to 30% are in the two plates. Reducing the electrolyte saturation of the AGM makes easier the O_2 transfer through the separator, but it hinders the movement of the H^+ and H_2O flows and it decreases the discharge capacity of the battery. Hence, the efficiency of the closed oxygen cycle and the discharge capacity of the cell depend on the properties of the AGM and on the design of the lead-acid cell.

The aim of this paper is to determine the influence of the compression of the active block, current density, temperature and number of cycles on the efficiency of the closed oxygen cycle of the VRLA batteries.

2. Experimental

2.1. Cell preparation

Commercial SLI positive and negative plates were used in this research. The AGM was 440 g/m^2 a product of Hollingsworth and Vose. The active block was designed with 4 positive and 5 negative plates. The AGM separator was 95% saturated with H_2SO_4 s.g. 1.29. The positive plates were wrapped with AGM separators.

2.2. Battery testing

Twelve V/42 Ah batteries were prepared. They were subjected to cycle life tests with a Bitrode NC system that allows individual cell testing with current up to 50 A. The charge CC-CU was common for all the cells of the battery. The charge parameters were:

(a) $I_1 = 22$ A up to $U_1 = 14.8$ V

(b) $U_2 = 14.8$ V to charge factor 110%

The discharge current was $I = 8.4$ A (5 h rate of discharge) down to a cut-off voltage of 1.70 V/cell. As any cell reached the latter value it was automatically switched off by the testing equipment and the discharge was continued for the other cells. The batteries were kept at a constant temperature of 25°C in water tanks. Periodically after a certain number of cycles the temperature was raised to 50°C for several cycles to eliminate the stratification of the electrolyte in the cells.

2.3. Determination of the closed oxygen cycle efficiency (ECOC)

In order to determine the efficiency of the COC, we created the following experimental method.

The oxygen flow I_{O_2} is generated at the positive plates. Part of this flow $(1-\theta)I_{O_2}$ reaches the negative plates and is reduced there. This part determines the closed oxygen cycle efficiency. Another part θI_{O_2} leaves the cell.

$$I_{O_2} = (1-\theta)\, I_{O_2} + \theta I_{O_2}$$

If the θI_{O_2} flow is high, this means that COC has low efficiency and vice versa. If we measure the rate of the O_2 flow leaving the cell (θI_{O_2}) we can estimate the COC efficiency.

Fig. 2 presents a conceptual scheme of the device that was invented for measuring the gas flow leaving the cell.

The device comprises two glass tubes (A and B) connected by a capillary. The tubes are half filled with water.

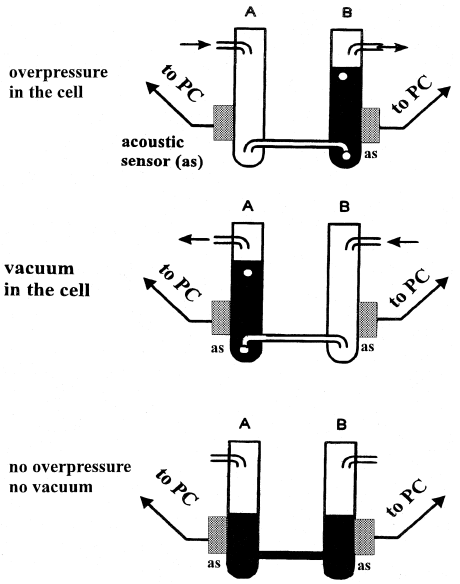

Fig. 2. Conceptual scheme of the device for measuring the gas flow leaving the cell.

One of the tubes (A) is connected to the cell and the other one (B) is open to the air. When the gas pressure in the cell increases, the evolved gas exerts a pressure on the water in the tube A. The water from the tube A passes into the tube B through the capillary. When the gas pressure in the cell becomes higher than the sum of the atmospheric one plus that of the water column in the tube B, the gas leaves the capillary in tube B in the form of bubbles. On detachment of a bubble from the capillary, a sound with a definite frequency is generated. There is an acoustic sensor attached to the tube that detects the sound of the bubble leaving the capillary. The electric signal generated in the sensor is transmitted to a computer where it is recorded and memorized. The volume of a bubble is determined experimentally. Through counting of the number of the bubbles formed per minute we determine the rate of the gas leaving the cell.

A second sensor is attached to tube A to measure the volume of gas that enters the cell when vacuum is created in it on discharge.

With the help of this device, we estimated the influence of different parameters on the efficiency of the closed oxygen cycle in lead-acid cells.

3. Results and discussion

3.1. Effect of the active block compression on the capacity and cycle life of VRLAB

Recently the role of the compression on the active block of the lead-acid battery has been a subject of intensive investigations [3–13]. The influence of this parameter on the capacity, life and on the ECOC was first established. For this purpose, we inserted 1 mm thick polyethylene sheets in a cell box. One such sheet exerts an AGM compression of 25%. In another cell, we inserted two polyethylene sheets thus applying a compression of 29.5% to the AGM, and the third cell was left without polyethylene sheets. The compression of the AGM in this cell was 20%.

These three cells were set to cycling and the capacity was measured at each cycle. Three times the battery obtained was heated to 50°C. Fig. 3 presents the cell capacity vs. the number of cycles. It can be seen that higher capacity and longer cycle life are delivered by cell 2 with an AGM compression of 25%.

Fig. 4 illustrates the change of the cell voltage and current during charge at the 27th, 57th and 77th cycles. The voltage curves of the cells with compression of 20 and 29.5% pass through a maximum between the first and second hours of the charge. This behavior is very clearly

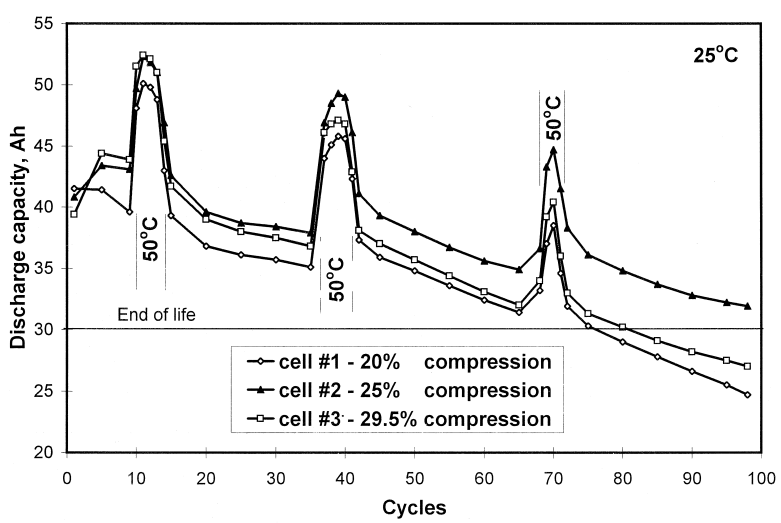

Fig. 3. Dependence of the discharge capacity of the three cells with different extent of compression on the number of cycles.

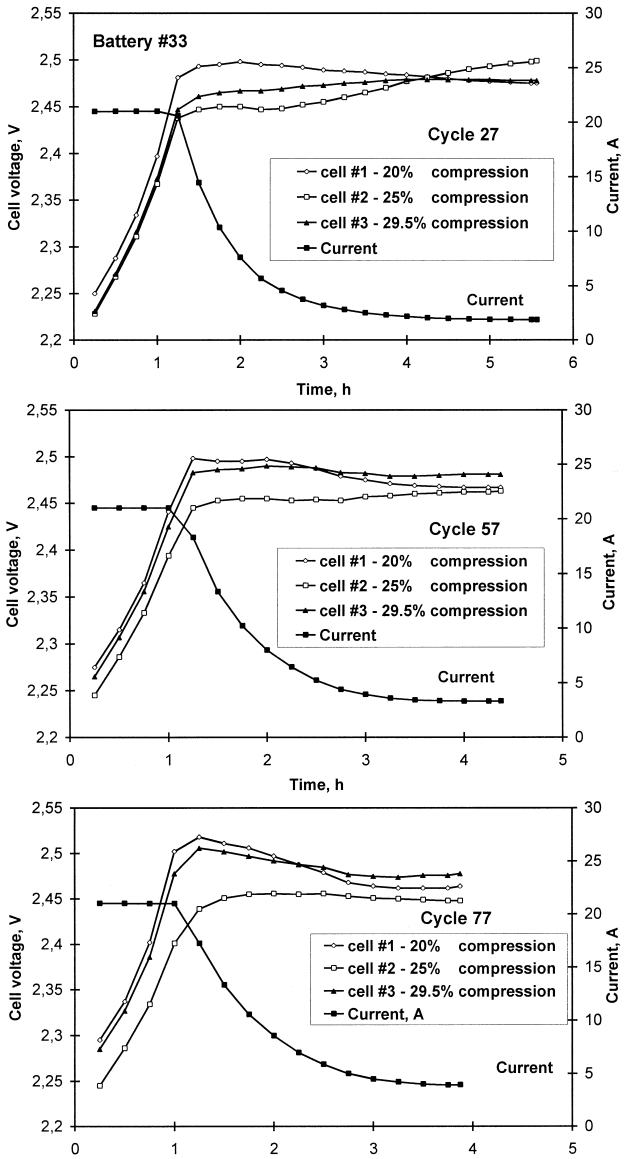

Fig. 4. Change of the cell voltage and current during charge.

expressed at the 57th and 77th cycles. The voltage curve of the cell with 25% compression rises to a certain value and that remains almost constant. These changes of the cell voltage with time are connected with both the processes of the charge of the active masses and the phenomena in the AGM.

Through measuring the rate of gas evolution from the cells ($V_{\text{out O}_2}$) at the 27th, 57th and 77th cycles during charge the ECOC was determined. Fig. 5 presents the results obtained. Fig. 6 presents the data of the total gas amount leaving each of the cells during the charge.

Fig. 5 shows that at the beginning of the charge (the efficient charge stage) the current mainly supports the progress of the electrochemical reactions of converting of $PbSO_4$ into Pb and PbO_2.After a certain period of time the processes of water decomposition start. A fraction of the gas generated leaves the cells. At the 27th cycle this process starts after 12 min of charge. At the 57th and the 77th cycles, it commences after the first 10 min of charge. For 30–40 cycles, the corrosion processes occurring at the positive grids have introduced into the positive active mass (PAM) enough ions of the alloying additives of the grid alloy (Pb — 1.8% Sb — 0.2% Sn — 0.15% As — 0.03% Se) that these cause the oxygen overvoltage to decrease. For this reason the second stage of the charge starts a bit earlier.

The curves $V_{\text{out O}_2}/t$ (Fig. 5) are generally characterized by a peak at the beginning and after a period of decline, by the appearance of a maximum. The peak can be connected with the following phenomenon. In spite of the fact that the saturation of the AGM with electrolyte is lower than 95% gas channels through the AGM separator do not exist at the beginning of the charge. The AGM contains electrolyte and separate, non-connected, gas bubbles. Forming of the gas channels through the AGM sheet is related to the overcoming of certain hindrances connected with pushing out the electrolyte from some of the AGM pores. This operation takes a certain period of time and requires a higher gas pressure formed at the positive plate/AGM interface. During this period it is easier for the gas to leave the cell and a peak in the curve $V_{\text{out O}_2}/t$ appears. The curve begins to decline when the gas channels are formed through the whole thickness of the separator and/or the voltage of the battery reaches 14.8 V and the current starts to decrease.

Let us analyze the changes of peak height with increase of the number of the cycles of the cells with different compression.

(1) Cell #1 — with compression 20%. The peak gets higher with the increase of the number of cycles, i.e., the formation of the gas channels in the AGM gets harder. Fig. 6 shows that, for 20% compression of the AGM, at the 27th cycle, the total amount of gas leaving the cell is less than that of the other cells, i.e., the ECOC is higher at this degree of compression. At the 57th and the 77th cycles, the total amount of gas leaving the cell during the charge is 465 ml and 478 ml respectively, and the heights of the peaks for the same cycles increase up to 260 ml/h and 315 ml/h. Hence, at this compression of the active block, such changes in the pore systems of the AGM, PAM and NAM occur that the resistance to creating the gas channels between the plates is increased and ECOC is lowered. All these phenomena proceed at a level of good ECOC.

(2) Cell #2 — with compression 25%. The height of the initial peak at the 27th cycle is similar to that of cell #1, but with increasing number of cycles it decreases, i.e., formation of the gas channels through the AGM separator is facilitated. Fig. 6 illustrates that the amount of gas evolved from the cell at the 27th cycle is twice that of cell #1. This means that even a 5% increase in the degree of compression reduces the ECOC substantially. It can be due to: (a) decreasing the radius of the pores; (b) decreasing the number of the pores with a large radius along which

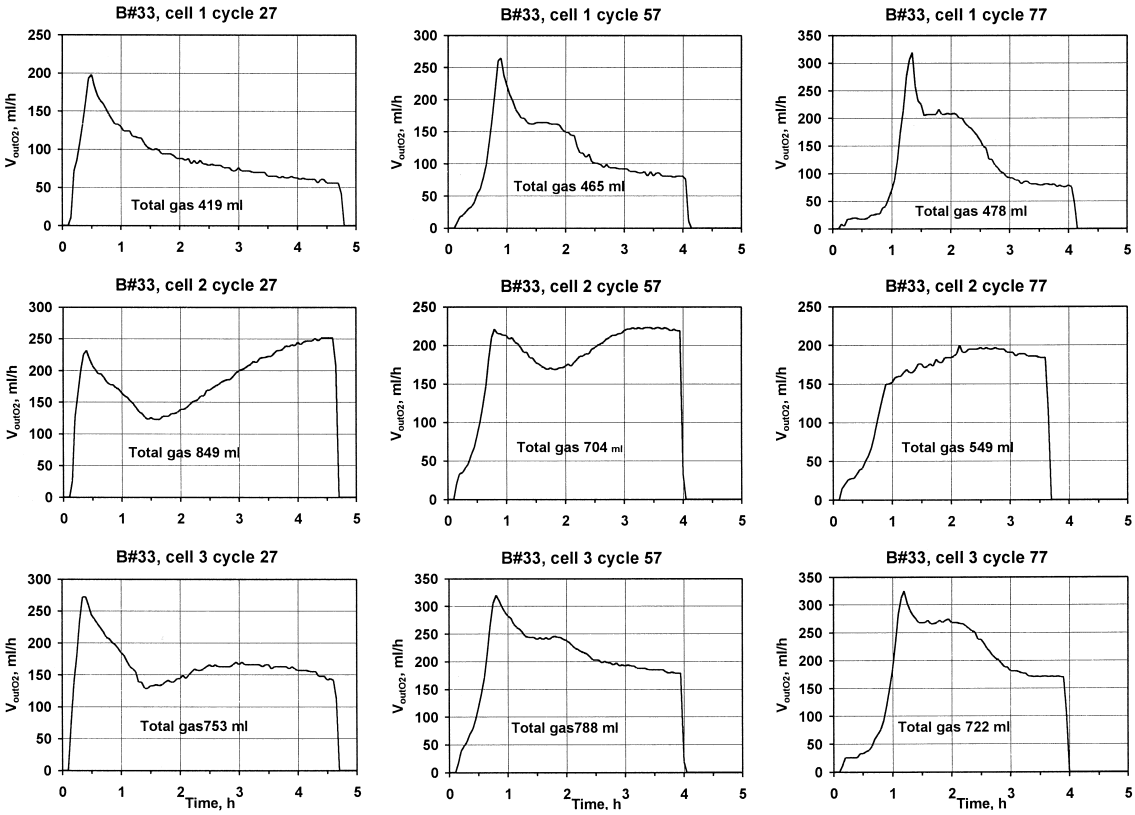

Fig. 5. Change of the rate of gas flows which leave the three cells during the charge at 27th, 57th and 77th cycles.

the gas moves through the AGM. It is known that the uncompressed AGM has a mean ''pore'' radius between 5 μm and 15 μm. The mean ''pore'' radius of the compressed AGM changes from 0.8 to 1.5 μm, depending on the degree of compression. Thus, the increase of the compression decreases the mean pore radius and hence the number of large pores along which the gas flows through the AGM separator. This lowers the ECOC but it can raise the state of charge of the negative plate and consequently increase the capacity of the cell. Fig. 6 shows that at the 57th and 77th cycles, the ECOC is strongly raised and the total amount of gas evolved from the cell is abruptly decreased. This compression changes the pore radius distribution and the pore volume in the AGM, PAM and NAM in such a manner that the ECOC is improved and the life of the cell is the longest (Fig. 4).

(3) Cell #3 — with compression of 29.5%. Fig. 5 shows a weak increase of the peak in the V_{outO_2}/t curve at cycling and Fig. 6 — a low ECOC which generally changes little with the number of cycles. This degree of compression is too high to allow favorable changes in the structures of the AGM, PAM and NAM to take place.

Fig. 5 illustrates that a broad maximum appears after the initial peak in the curve $V_{\mathrm{out\ O}_2}/t$. The disposition and size of the maximum depends on the compression of the active block and on the number of cycles. No maximum is observed at the 27th cycle of cell #1. It appears at the 57th cycle and increases at the 77th cycle. This maximum is clearly seen at the 27th cycle of cell #2 and at the 77th cycle it even merges with the peak. In the case of cell #3 the maximum is wide and moves towards the beginning of the charge with increasing number of cycles. It is difficult to explain definitely the appearance of the maximum based on this research only.

It is known that in spite of the fact that COC keeps the potential at the negative plate low, hydrogen still evolves

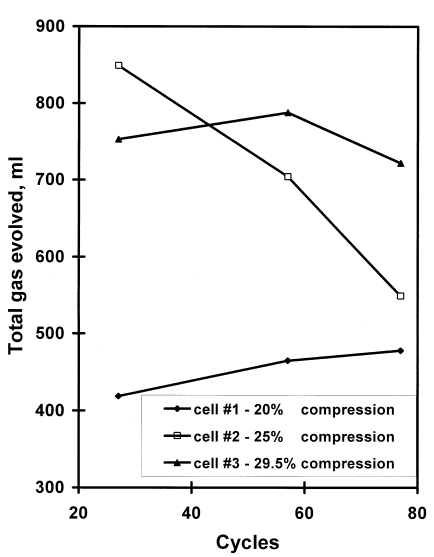

Fig. 6. Total gas volume evolved from the three cells during the charge at 27th, 57th and 77th cycles.

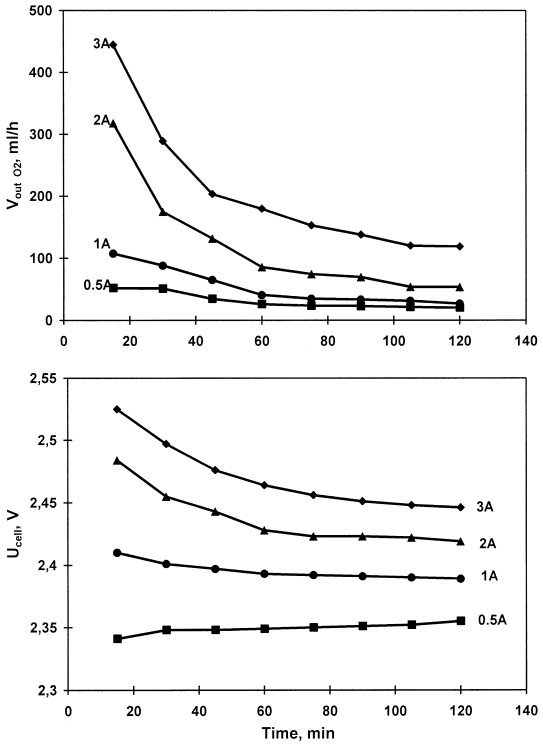

Fig. 7. Changes of the cell voltage and the rate of the gas flow which leaves the cell during charge.

to some extent. This may influence the form of the $V_{out\ O_2}/t$ curve.

3.2. Effect of current density (O_2 flow) on cell polarization and on ECOC

The experiment was performed using a 12 V/42 Ah VRLA battery. The rate of the oxygen evolution was measured during the overcharge period when only the reaction of oxygen evolution proceeds. Fig. 7 presents the changes in the cell voltage and in the rate of oxygen leaving the cell ($V_{out\ O_2}$) during 3 h of polarization with different values of charge current.

From the data in the figure the following conclusions can be drawn.

(1) The changes in the cell voltage and in the $V_{out\ O_2}$ with time are analogous. Therefore we can assume that polarization of the cell depends on the hindrances appearing in the transport of the oxygen through the AGM.

(2) At the beginning of the polarization, when the oxygen evolution starts, the cells are in a non-steady state. After a certain period of time (1 to 2 h) a steady state of efficiency of the COC and of the cell voltage is reached.

(3) At the steady state of the cell (for example at 120 min), the voltage of the cell and $V_{out\ O_2}$ increase with the increase of the current.

Fig. 8 presents the dependence of the stationary values of $V_{out\ O_2}$ on the cell voltage.

A linear dependence of $V_{out\ O_2}$ on the polarization of the cell is observed in an interval of the current values (0.5–2.0 A). As a critical value of the current is reached (i.e., of the O_2 flow) an abrupt decline in the efficiency of the COC (increase of $V_{out\ O_2}$) starts. This shows that the maximum possibility for the AGM to transport oxygen between the plates is reached. Any further increase of the current leads to an increase of the pressure in the cell and of the flow of gas leaving the cell. Consequently, using this limiting parameter $(i_{lim})_{AGM}$, it is possible to characterize the features of the AGM related to its ability to support O_2 flow. This parameter may be related to the maximum number of gas channels that are formed in the AGM along which the

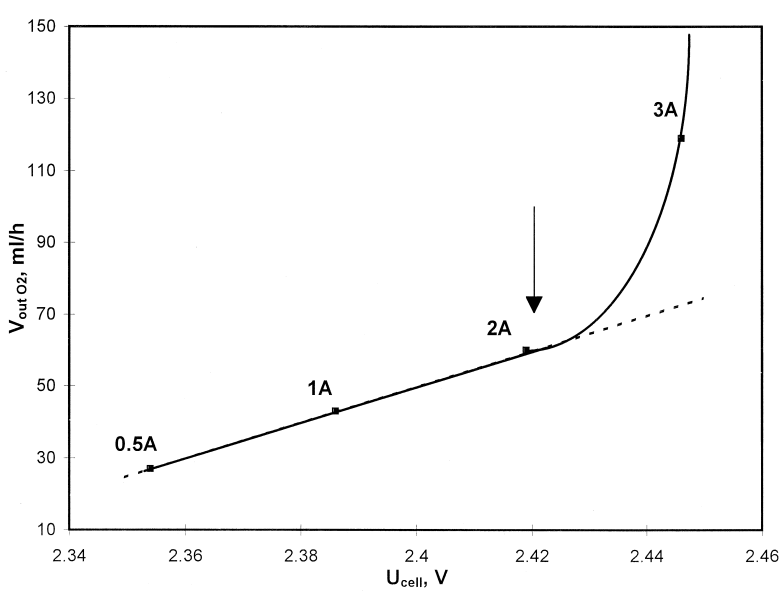

Fig. 8. Dependence of the rate of the stationary gas flow leaving the cell on its voltage.

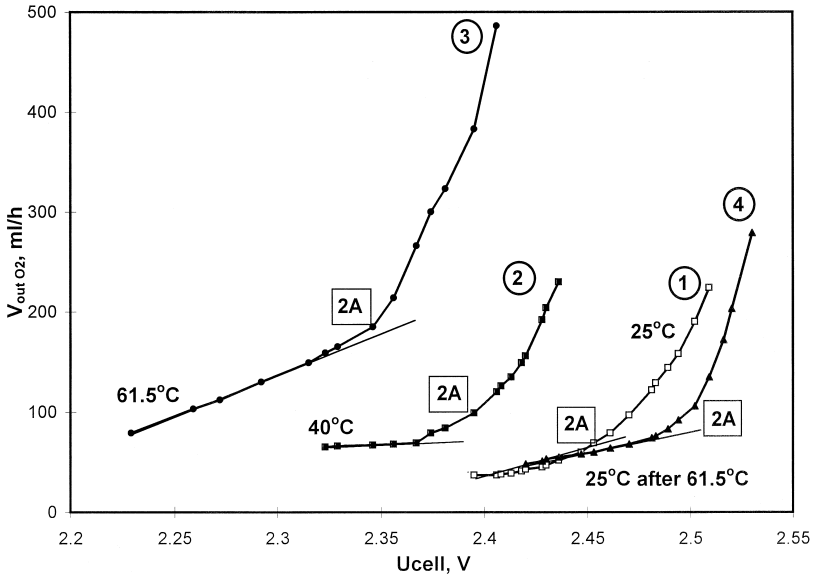

Fig. 9. Dependence of the rate of the stationary gas flow leaving the cell on its voltage at different temperatures.

O_2 flows between the positive and the negative plates. This critical value depends on the structure of the AGM and on the degree of AGM saturation with electrolyte. In the case with the cell whose data are presented in Fig. 8, this limiting current is 2 A and that corresponds to 0.05 C_{20} A.

3.3. Effect of temperature on the efficiency of the COC

Twenty-five charge–discharge cycles were carried out first. Then the battery was charged and the investigation was carried out in the third period when only the reactions of the COC proceed. We followed the dependence of the rate of gas leaving the cell ($V_{\text{out } O_2}$) and the cell voltage during the stationary period at different temperatures. The value of the current was increased after every 2 h of polarization. The results are presented in Fig. 9. First the $V_{\text{out } O_2}/U_{\text{cell}}$ dependence was plotted at 25°C (curve 1), then at 40°C (curve 2) and finally at 61.5°C (curve 3). Then the temperature was reduced to 25°C and again $V_{\text{out } O_2}/U_{\text{cell}}$ dependence (curve 4) was determined to assess the reversibility of the AGM properties and structure.

Let us consider the behavior of the cell at $I = 2$ A. It can be seen that with increase of temperature the polarization of the cell decreases and so does the efficiency of the COC (the value of $V_{\text{out } O_2}$ rises). Besides, the critical value of the current at which $V_{\text{out } O_2}$ starts to raise quickly decreases with increasing temperature. This means that the ECOC reduces with increasing temperature. If we compare curves 1 and 4 we can see that they differ in profile. This indicates that during the rise onto higher temperature, the structure of the AGM changes.

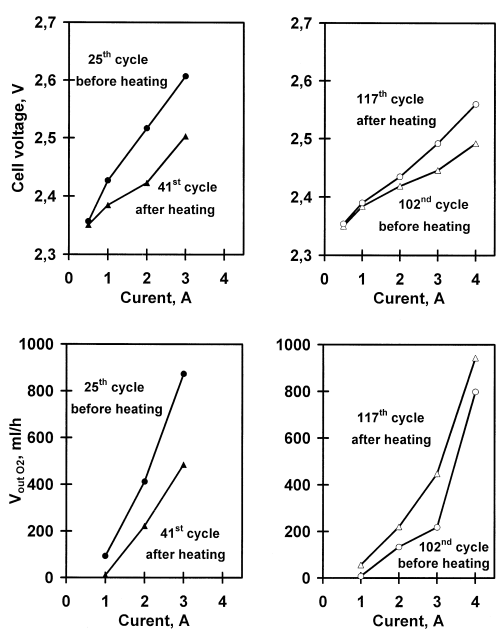

Fig. 10. Dependence of the cell voltage and the rate of the gas flow leaving the cell on the current at different numbers of charge–discharge cycles.

3.4. Effect of cycling and temperature on the U_{cell}/I and $V_{\text{out } O_2}/I$ dependencies determined during the period of water decomposition

The cycling was carried out at 80% DOD. Twice (between the 30th and the 33rd and between the 110th and the 112th cycles), the battery was heated at 50°C. At the 25th and the 41st cycles (before and after the first heating) and at the 102nd and the 117th cycles (before and after the second heating), the efficiency of the COC and the cell voltage with the change of the current were determined. The results obtained are presented in Fig. 10.

The polarization dependence $U_{cell} = f(I)$ and the dependence $V_{out\ O_2} = f(I)$ are influenced by the thermal treatment of the AGM and the number of the cycles. At the beginning of cycling (25–40 cycles) heating of the battery causes the cell polarization to decrease and the efficiency of the COC to increase. After 100 cycles heating of the battery increases slightly the cell polarization and decreases the efficiency of the COC. This behavior shows that at heating and cycling the physical and chemical properties of the AGM are changed substantially.

4. Conclusions

On the grounds of the experimental results obtained the following general conclusions can be made.

(1) The discharge capacity and cycle life of the VRLA batteries depend on the compression of the active block. The maximum capacity and longest cycle life have been achieved at 25% AGM compression. The efficiency of the COC decreases at a higher AGM compression.

(2) The AGM has a dynamic structure with a pore system that changes under the action of the temperature, O_2 flows (current), compression and the number of charge–discharge cycles.

(3) The AGM has a limited number of gas channels along which the O_2 flows between the two plates. This number depends on the AGM structure and the degree of saturation with electrolyte. Hence, there is an upper limit of the rate of recombination determined by the AGM.

(4) The efficiency of the COC decreases with an increase of the temperature.

(5) The efficiency of the COC increases at the beginning of the cycling and after certain number of cycles it starts to decrease. This behavior is related to the chemical and mechanical stability of the AGM.

References

[1] D.H. McClelland, J.L. Devitt, US Patent 3,862,861, 1972.
[2] D. Berndt, Maintenance-Free Batteries, Research Studies Press, Wiley, New York, 1993, p. 112.
[3] K. Takahashi, M. Tsubota, K. Yonezu, K. Ando, J. Electrochem. Soc. 130 (1983) 2144.
[4] J. Alzieu, J. Robert, J. Power Sources 13 (1984) 93.
[5] J. Alzieu, N. Koechlin, J. Robert, J. Electrochem. Soc. 134 (1987) 1881.
[6] S. Atlung, B. Zachau-Christiansen, J. Power Sources 30 (1990) 131.
[7] D. Pavlov, J. Power Sources 33 (1991) 221.
[8] J. Landfors, J. Power Sources 52 (1994) 99.
[9] A.F. Hollenkamp, R.H. Newnham, J. Power Sources 67 (1997) 27.
[10] G. Zguris, J. Power Sources 67 (1997) 307.
[11] M. Calábek, K. Micka, P. Baca, P. Krivák, L. Sácha, J. Power Sources 78 (1999) 94.
[12] L.T. Lam, H.P. Haigh, O.V. Lim, D.A.J. Rand, J.E. Manders, J. Power Sources 78 (1999) 139.
[13] A.L. Ferreira, Battery Man, May issue (1999) 70.